Electronic Supplementary Material (ESI) for Physical Chemistry Chemical Physics.

Supporting Information for

Topology induced Crossover between Langevin, Subdiffusion, and Brownian Diffusion Regimes in Supercooled Water

Kaicheng Zhu, Saber Naserifar, William A. Goddard III, and Haibin Su

Corresponding authors: William A. Goddard III; Haibin Su
Email: wag@caltech.edu; haibinsu@ust.hk

This PDF file includes:

1. Molecular Dynamics Simulations of Supercooled Water

The Molecular Dynamics (MD) simulations were performed using RexPoN Force Field with rigid and flexible water models to compute entropy and diffusivity at various temperatures. The mathematical formulation of RexPoN, training set, optimization process, and complete list of parameters are provided separately[1]. We integrated the RexPoN Force Field into the LAMMPS[2] MD simulator package, which we used for all simulations.

All simulations used periodic cells with 216 rigid molecules. All supercooling simulations were carried out in the *NVT*-MD ensemble along the 1 atm density line. The experimental densities were used for temperatures above 240 K while for temperatures below 240 K, we used the extrapolation of Kim *et al*[3]. For each density, we first equilibrated the system at 300 K for 1 ns using rigid water model. Then, the system was cooled down during a step-by-step process to 298, 273, 260, 250, 240, 235, 232, 230, 228, 225, 220, 210, and 200 K. At each temperature, the system was relaxed for 0.5 ns before going to the next temperature. The simulation time step was 1.0 fs. To control the temperature, we used the Nosé-Hoover thermostat with a relaxation time of 100 fs[4]. To compute the MSD data, we continued the *NVT*-MD simulations for another 1 ns but using flexible water model while using used Langevin thermostat[5] with damping of 100 fs to control the temperature of flexible water. In our earlier papers we found that flexible waters are necessary to obtain accurate diffusion properties[6], and we also showed that using a flexible water model requires a smaller r simulation time step (order of 0.1 fs) to fully equilibrate the water system. This is known to be due to very fast movement of hydrogen atoms in the system and nuclear quantum effects (NQE). Regarding NQE, we find that much smaller time steps (in order of 0.01 fs) might be needed[7]. Therefore, performing flexible supercooled water simulations for a wide range of temperatures and for nanoseconds (required to equilibrate the systems) would be computationally very demanding. Thus, we first equilibrated the systems with rigid water (which gave excellent thermodynamic properties) and then switched to flexible simulations to capture different diffusion modes of water molecules. We used Langevin thermostat for flexible water because we noticed that this thermostat allows better equilibration between translational, vibrational, and rotational modes of water. This helped to control the temperature of water molecules for the above modes

homogenously throughout the simulations. For 200 K, we ran the simulations for 2 ns to produce enough trajectories for the MSD plot in the Brownian regime.

2. Brief Overview about RexPoN Force Field

The previous publications about RexPoN Force Field compared in detail its accuracy for MD simulations for water systems against experiment and against well-known water models including MB-pol, CC-pol, TIP3P, TIP4P-2005, SPC/E, ST2, and DFT methods such as PBE, PBE-D3, and SCAN.

Indeed, we find that RexPoN Force Field provides the most accurate description of water properties. We compare predicted properties using RexPoN Force Field with experiment and with QM MD and other Force Fields as follows.

RexPoN predicts:

- A melting point (T_{melt}) between 273 and 273.5 K, very close to the experimental value of 273.15 K. This can be compared to T_{melt}=263.5K for MB-Pol, 420 K for PBE DFT, 146 K for TIP3P; and 215 K for SPC/E.
- A density of 0.9965 gr/cm^3 at 298 K, agreeing exactly with experiment (it also captures the maximum density of 1.000 gr/cm^3 at 4 C°). This can be compared to 1.007 for MB-Pol, 0.944 gr/cm^3 for PBE DFT, and 1.05 for SCAN DFT.
- A heat of vaporization of 10.36 kcal/mol, low by 0.16 kcal/mol from experiment. This can be compared to 10.93 for MB-POL, 6.2 kcal/mol for PBE DFT.
- An entropy at 298 K of 68.4, low by 2%. This can be compared to 51.32 for PBE DFT.
- A dielectric constant at 298 K of 76.1, low by 3%. This can be compared to 68.4 for MB-POL, and 112 for PBE DFT.

Of most interest is the oxygen-oxygen radial distribution function (g_{OO}) from RexPoN. The predicted g_{OO} for the first peak (ending at 3.43 Å) is in agreement with experiment with a slight shift in the peak position from 2.86 Å to 2.84 Å and the peak height from 2.50 to

2.34. In addition, the computed coordination number, N_{OO}=4.7 is in good agreement with experiment, N_{OO} = 4.5.

We provided many more details about the accuracy of the RexPoN Force Field in Naserifar *et al.*[1], and more discussions about the comparison of the RexPoN Force Field with other models in Naserifar *et al.*[7]. We explained there that the spectacular agreement with experiment indicates that RexPoN describes accurately the structure of water, especially the first shell. We discussed how the inaccuracy of other water models have affected their predictions for the structure of the first coordination shell, coordination number at the first minimum of g_{OO}, and number of strong hydrogen bonds in liquid water.

3. Characterization of Strong Hydrogen Bond

The strong hydrogen bond analysis was performed based on r_{OO} =2.93 Å cut off distance, based on the equilibrium distance for water dimer. We used this cut off distance since it is the well depth of water dimer (4.98 kcal/mol). We have shown previously[7] that using other criteria (e.g. angle criterion[8] or defined strong hydrogen bond zone by DFT[9]) does not produce different results compared to the method used here.

4. Calculation of Dynamic Entropy

The dynamic entropies for all temperatures were computed with the 2PT technique[10–12]. The 2PT methodology is based on computing Fourier transform of the velocity autocorrelation function to calculate the vibrational density of states. The corrections are made for the diffusional contributions to achieve a finite density of states at ν=0. We used the last 100 ps of the MD trajectories at each temperature to compute the entropy for different time intervals to show the entropy production dynamics, as denoted by the data points in Fig. 4(c). The 100-ps trajectories are divided into different groups of separate short trajectories of lengths varying from 100 fs to 20 ps. The vibrational density of states is calculated from transient trajectories of corresponding time intervals and averaged over

the 100-ps period. The thermal fluctuation at different time intervals is characterized by the temperature analysis, as shown in Fig. S4. The maximum relative difference is below 0.15% and the maximum relative standard deviation is below 2.5%.

In the statistical analysis of transient kinetic entropy, we use the 100-fs time interval to conduct 2PT calculation. We see a clear pattern that within the timescale of 100 fs (i.e., before the HB network relaxes), the molecular translational entropy preserves its self-correlation. This is because within this timescale, the local HB network feature coupled with a single water molecule is generally maintained. So, the time interval of the trajectories used to calculate the kinetic entropy should not exceed the timescale around 100 fs. Because the relative accuracy of the calculated entropy reduces with a decreasing time interval, we use the calculated entropy data of 100-fs intervals, which is less than γ_{ϕ}^{-1}.

5. Multi-Modality Test of Entropy Distribution

To validate the three-component behavior of the kinetic entropy of the water molecules, we conducted the calibrated Silverman's test to check the multi-modality of the entropy distribution data[13,14]. Since the distributions of entropy clearly show non-single-Gaussian behavior, the number of statistical modes of interest was set to vary from 2 to 4. Thus, the calibrated Silverman's test was done under the condition of k=2, 3, and 4, with the number of bootstrap replications set to 2000. The p-values of the Silverman's test results at all temperatures are shown in Fig. S3. Although the exact accuracy is limited by the fluctuation of the test result, the robust pattern supports our three-component analysis and the three-state model: the k=3 curve is the dominant throughout the temperature from 230 to 298 K, where the three states co-exist because their free energy differences are relatively small in this region. On the other hand, the k=2 curve dominates the low temperature region from 200 to 220 K, where the TRS state takes little partition due to its high free energy under this circumstance and only the 1D and 2D states share the main statistical significance.

6. Ring Statistics of Hydrogen-Bond Network Topology

Thanks to the recent advances of methodologies to study the topological networks in materials, we could perform ring analysis to characterize the hydrogen bond network in supercooled water by quantitative manners. The systematic statistics of rings has gone beyond the first and second coordination shells to describe the network topology at the intermediate and long-range scales in amorphous systems.

Various methods of defining a ring have been developed, e.g., the King's method which defines a ring based on the shortest path that comes back to the starting node (i.e., water molecule) through its nearest neighbors, and the SP method where a ring is defined based on the shortest path the connects the two nearest neighbors.

A ring is defined as primitive or irreducible if it cannot be reduced into two smaller rings. In our previous paper where the 1D-2D topological transformation was explained by ring analysis, only primitive rings were considered. Further details are provided elsewhere[6].

The number of n-membered (n=5, 6, or 7 in our previous analysis) rings changes with temperature for supercooled water from 200 to 298 K. For all cases, the number of rings increases as the temperature is decreased. We found there is a clear jump in the number of rings when temperature varies from the 228 K to 235 K where the topological transformation takes place.

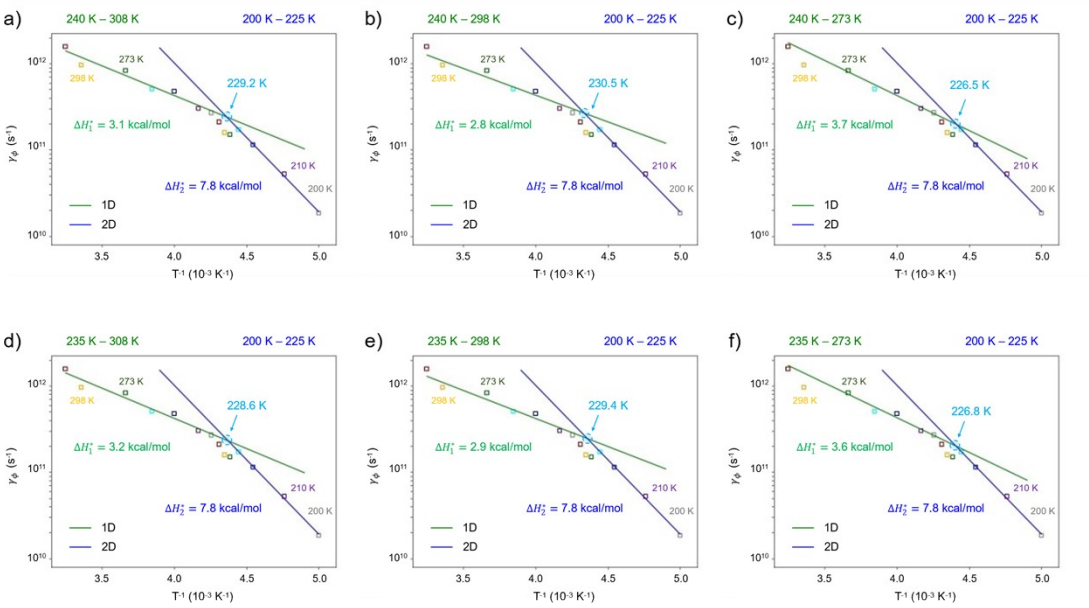

Figure S1. Two separate activation processes, at low-temperature (below 230 K) and high-temperature (above 230 K) regions, indicate the transition at around 230 K. From (a) to (f), the exact values of the transition temperature and related activation enthalpy are shown when different sampling regions are used to quantify the activation processes. The transition temperature varies from 226.5 K to 230.5 K, and the activation enthalpy varies from 2.8 kcal/mol to 3.7 kcal/mol.

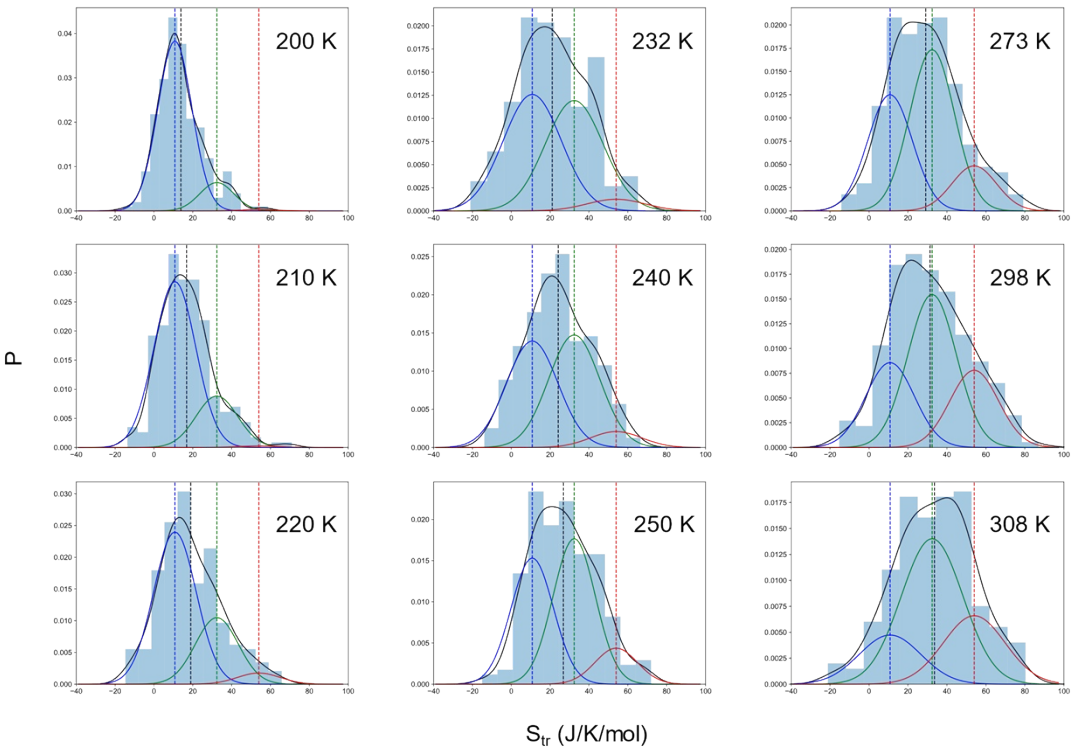

Figure S2. The probability distribution of translational kinetic entropy decomposed into three distinct components from 200 K to 308 K. The blue, green, and red vertical dash lines denote the separate mean values for the low-, middle- and high-entropy groups, and the black denote the systematic mean value of the kinetic entropy for all water molecules.

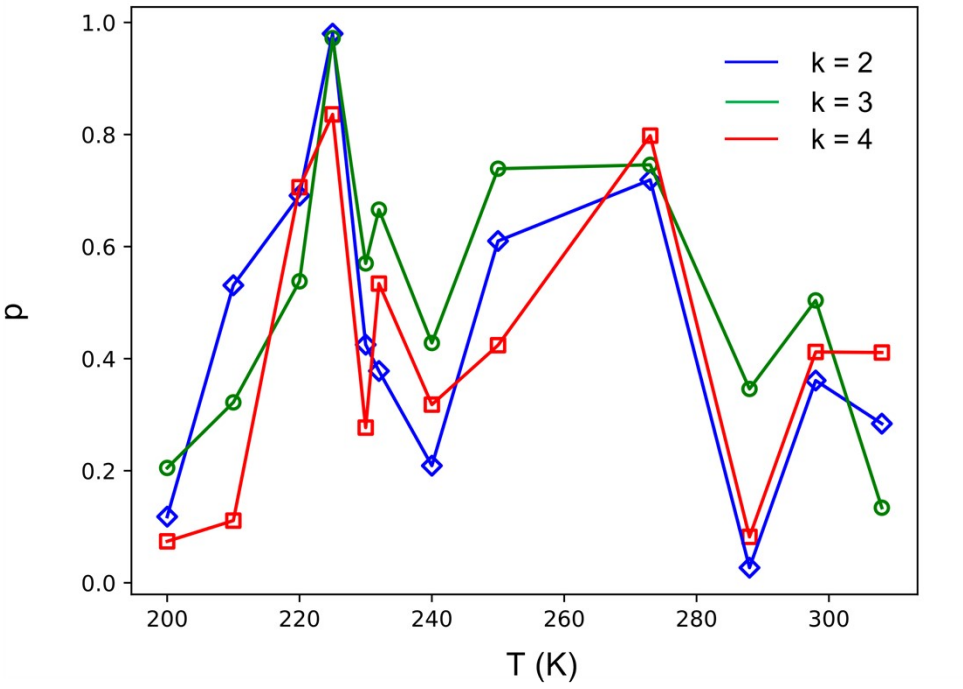

Figure S3. Calibrated Silverman's tests of the multi-modality of the entropy distribution from 200 to 308 K. The p-values of the tests with the modality number of k=2,3, and 4 are shown at various temperatures. The supremacy of k=3 remains from 230 to 298 K, and k=2 case has the highest p-value from 200 to 225 K.

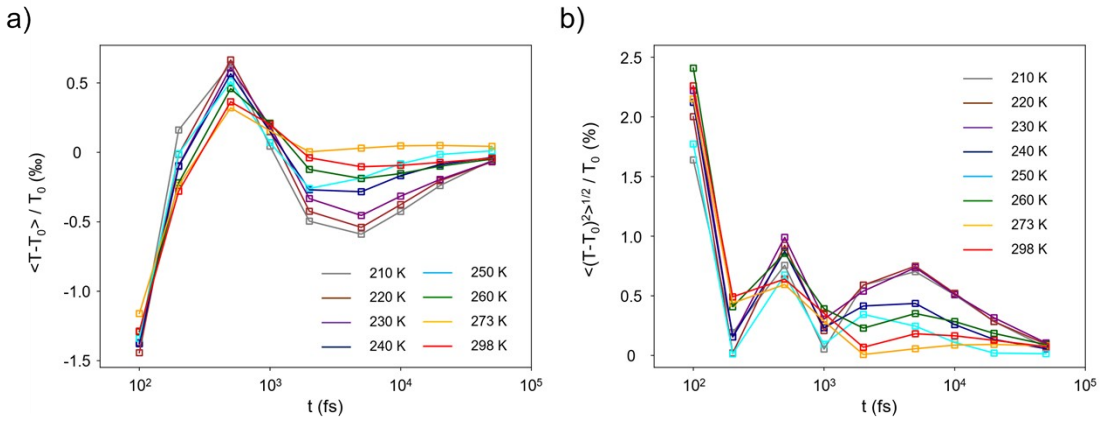

Figure S4. Temperature fluctuation calculated from MD trajectories of different time intervals. The last 100-ps MD trajectories are separated into groups of transient trajectories of corresponding time intervals from 100 fs to 50 ps. Temperature is computed based on kinetic energy and averaged over all transient trajectories with the same time intervals. (a) Relative temperature difference. (b) Relative standard deviation of temperature fluctuation.

References

1. Naserifar, S. & Goddard, W. A. The quantum mechanics-based polarizable force field for water simulations. *J. Chem. Phys.* **149**, 174502 (2018).
2. Plimpton, S. Fast Parallel Algorithms for Short-Range Molecular Dynamics. *J. Comput. Phys.* **117**, 1–19 (1995).
3. Kim, K. H. *et al.* Maxima in the thermodynamic response and correlation functions of deeply supercooled water. *Science* **358**, 1589–1593 (2017).
4. Nosé, S. A unified formulation of the constant temperature molecular dynamics methods. *J. Chem. Phys.* **81**, 511–519 (1984).
5. Schneider, T. & Stoll, E. Molecular-dynamics study of a three-dimensional one-component model for distortive phase transitions. *Phys. Rev. B* **17**, 1302–1322 (1978).
6. Naserifar, S. & Goddard, W. A. Anomalies in Supercooled Water at ∼230 K Arise from a 1D Polymer to 2D Network Topological Transformation. *J. Phys. Chem. Lett.* **10**, 6267–6273 (2019).
7. Naserifar, S. & Goddard, W. A. Liquid water is a dynamic polydisperse branched polymer. *Proc. Natl. Acad. Sci.* **116**, 1998–2003 (2019).
8. Jeffrey, G. A. *An Introduction to Hydrogen Bonding*. (Oxford University Press, 1997).
9. Wernet, P. *et al.* The Structure of the First Coordination Shell in Liquid Water. *Science* **304**, 995–999 (2004).
10. Lin, S.-T., Blanco, M. & Goddard, W. A. The two-phase model for calculating thermodynamic properties of liquids from molecular dynamics: Validation for the phase diagram of Lennard-Jones fluids. *J. Chem. Phys.* **119**, 11792–11805 (2003).
11. Lin, S.-T., Maiti, P. K. & Goddard, W. A. Two-Phase Thermodynamic Model for Efficient and Accurate Absolute Entropy of Water from Molecular Dynamics Simulations. *J. Phys. Chem. B* **114**, 8191–8198 (2010).
12. Pascal, T. A., Schärf, D., Jung, Y. & Kühne, T. D. On the absolute thermodynamics of water from computer simulations: A comparison of first-principles molecular dynamics, reactive and empirical force fields. *J. Chem. Phys.* **137**, 244507 (2012).

13. Silverman, B. W. Using Kernel Density Estimates to Investigate Multimodality. *J. R. Stat. Soc. Ser. B* **43**, 97–99 (1981).
14. Hall, P. & York, M. ON THE CALIBRATION OF SILVERMAN'S TEST FOR MULTIMODALITY. *Stat. Sin.* **11**, 515–536 (2001).